A scanning tunneling microscopy study of a new superstructure around defects created by tip–sample interaction on 2H- $NbSe_2$

2009 J. Phys.: Condens. Matter 21 265005

(http://iopscience.iop.org/0953-8984/21/26/265005)

J. Phys.: Condens. Matter **21** (2009) 265005 (8pp) doi:10.1088/0953-8984/21/26/265005

A scanning tunneling microscopy study of a new superstructure around defects created by tip–sample interaction on 2H-$NbSe_2$

Hui Wang[1,2], **Jonghee Lee**[1,2,3], **Michael Dreyer**[2] **and Barry I Barker**[2]

[1] Department of Physics, University of Maryland, College Park, MD 20742, USA
[2] Laboratory for Physical Sciences, 8050 Greenmead Drive, College Park, MD 20740, USA

E-mail: wanghui@lps.umd.edu

Received 2 March 2009, in final form 20 May 2009
Published 11 June 2009
Online at stacks.iop.org/JPhysCM/21/265005

Abstract

A low temperature scanning tunneling microscope (LT-STM) was used to investigate a new superstructure on the cleaved surface of a 2H-$NbSe_2$ single crystal after introduction of structural defects through bias voltage pulses during tunneling at 4.2 K. A charge density wave (CDW) with a $\sqrt{13} \times \sqrt{13}$ reconstruction was observed in the vicinity of the defects and the well-known 3×3 CDW was observed far from these defects. Multiple layers inside the defects were also exposed and showed the new modulation of the CDW on all of the Se layers. This indicates a local 2H to 1T phase transition for the $NbSe_2$ crystal structure. Two other interesting observations are also included: a disordered CDW-like phase of the $\sqrt{13} \times \sqrt{13}$ structure near the atomic steps and an anomalous distortion in the underlying atomic lattice revealed by STM images. A local heating mechanism is proposed to explain the creation of these novel structures.

(Some figures in this article are in colour only in the electronic version)

1. Introduction

Charge density wave (CDW) states in quasi-2D systems such as transition-metal dichalcogenides continue to attract a great deal of interest [1, 2] especially with scanning tunneling microscopy (STM) techniques [3, 4]. 2H-$NbSe_2$ is a well-studied example of this class of material. As described in [3], clear 3×3 atomic modulation on the surface revealed by STM in the topographic image and the energy gap in the differential conductance spectra agree well with theories of CDW in quasi-2D systems. This type of CDW is what we generally observe on the surface of the 2H (trigonal prismatic coordination) phase of dichalcogenides [4]. Another type of surface modulation was observed in Ag-doped 2H-$NbSe_2$ at room temperature [5]. A localized version of this modulation also exists in pure samples at room temperature [6] and at 4.2 K [7]. This new CDW modulation exhibits a $\sqrt{13} \times \sqrt{13}$ structure which is typically found in the 1T (octahedral coordination) phase of dichalcogenides [8]. The formation mechanism of this new CDW in 2H materials is unresolved.

In this paper we will show that we can create this new modulation by a controlled tip–sample interaction at 4.2 K and examine the atomic structure of the modulation in detail by STM. By applying a sudden change in the bias voltage or using a short period voltage pulse superimposed on the bias voltage, we can create a local structural defect, a 'pit', on the atomically flat surface of 2H-$NbSe_2$. As depicted in figure 1, the size of the defect is of the order of 100 nm in diameter and 10 nm in depth. A clean $\sqrt{13} \times \sqrt{13}$ superstructure is found around the edge and inside the defect. This method is reproducible and the new structure is stable during scanning at 4.2 K in our system. We are able to characterize it both on large and atomic scales. The voltage pulse method has been employed by others to generate structural defects on transition-metal dichalcogenides such as WSe_2 [9]. The voltage jump method was also used to generate similar surface modulation

[3] Present address: Department of Material Science and Engineering, University of Maryland, College Park, MD 20740, USA.

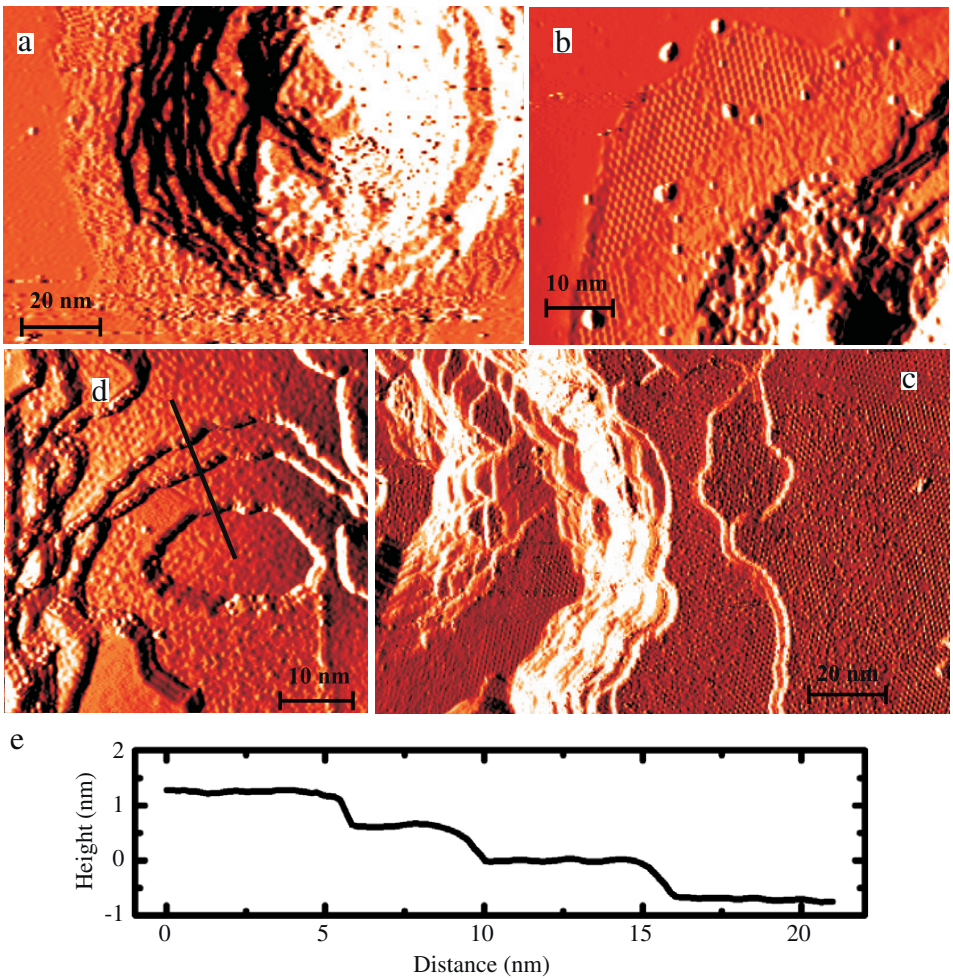

Figure 1. The defect and its vicinity. The defect created by a bias voltage jump. The electrons were moving from the tip to the sample. (a) An example to show the typical topographic profile of the defect and its vicinity. New modulation can appear in the rough area surrounding and inside the defect, which is demonstrated in (b)–(d). (b) Zoomed in to a corner of a defect. The regular lattice structure on the side is the new modulation. (c) A topographic profile on the side of another defect. It clearly shows the CDW on each sandwich layer exposed. (d) The topographic image of the bottom of a defect. The new modulations appeared on various layers. (e) The height measurement of the line cut made in (c). The heights of layers indicate that the exposed layers are all Se layers (see the text).

in 2H-$TaSe_2$ [10] and it was proposed that only the top Se layer had shifted. Our data indicate, however, a quasi-3D structural transformation that extends across multiple atomic layers.

We observed two novel features that are unique to this local modulation. The first is a order/disorder phase separation of the new modulation. A disordered phase was first seen in the silver-doped material [5], but was not reported in the local case [6] as well as in the 1T system [1]. This new phase suggests a localized CDW state. The second feature is an anomalously large atomic lattice distortion revealed by examining the atomically resolved images in the ordered region. The distortion in the unit cell of the $\sqrt{13} \times \sqrt{13}$ superstructure is much larger than the distortion in the usual 1T case. To the best of our knowledge this is the first time that detailed periodic structural displacements (PSD) of the CDW are revealed by STM. We propose that local heating generated this new modulation, in a process similar to spot welding [11] where the probe is brought close to the metal so the resistance is small and the heating is localized. We argue that a short pulse can generate enough heat locally to raise the temperature enough to induce a phase transition. In section 2, we will describe the experimental method and the general results. The two observations will be discussed in sections 3 and 4. We will summarize the paper in section 5.

2. Defect structure and the new modulation

The experiment was carried out using our home-built LT-STM. A pristine single crystal of 2H-$NbSe_2$ was cleaved at room temperature in a high vacuum of about 10^{-7} mbar. Then it was transferred to the STM in the LT chamber at 4.2 K within a few minutes. We prepared the chemically etched tungsten tip in the STM before transferring the sample by field emission against a single crystal of gold. The 2H phase of the crystal was confirmed by the observation of the 3×3 modulation on the atomically resolved surface. We used two different methods to generate the structural defect on the surface. In the first method, with the STM feedback turned on, we generated a short bias voltage pulse with a duration of 100 μs and an amplitude of 3–5 V. The bias voltage was set to 50–100 mV with a tunneling current of 0.1 nA before pulsing. The second

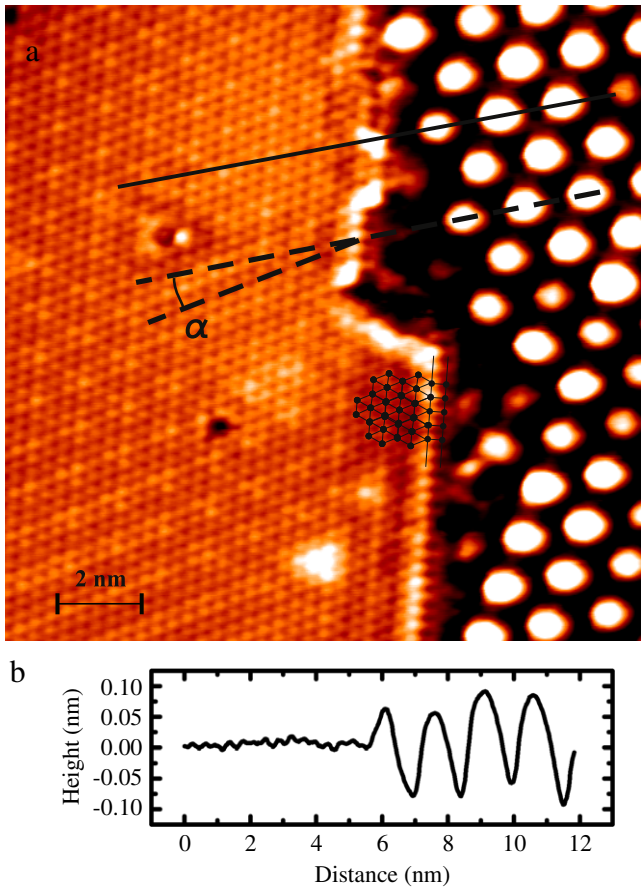

Figure 2. The interface of the two CDWs. The interface between the 3×3 CDW and the $\sqrt{13} \times \sqrt{13}$ CDW. In (a), the left shows the typical atomic lattice of the Se layer and the 3×3 CDW signature. On the right the big bubbles are the new modulation with a $\sqrt{13} \times \sqrt{13}$ construction. The lattice of the new CDW is rotated by an angle α with respect to the underlying atomic lattice. α was measured to be 13.9°. The atomic structure at the interface is illustrated by the lattice lines drawn upon the bright atom signatures. It shows a rectangular interface lattice. (b) The height measurement along the line cut (the solid line in (a)) across the interface.

method simply stepped the bias voltage from 3–10 mV to 5–10 V while scanning with the feedback on. This sudden change of bias voltage proved to be more reliable. We find that the critical voltage depends on the initial tunneling resistance. The higher the resistance, the larger the critical voltage needed to create the defect. For an initial voltage of 3 mV and tunneling current of 0.1 nA, the critical voltage is ∼5 V. For an initial voltage of 5 mV and tunneling current of 0.1 nA, the critical voltage is ∼10 V. We also tried using mechanical contact to create defects. We turned off the feedback and pushed the tip into the surface by increasing the z voltage on the piezo-tube scanner. No $\sqrt{13} \times \sqrt{13}$ modulation was found in the vicinity of defects created by this method. This excludes mechanical contact as a cause for the formation of the new CDW. All images shown in this paper were taken with a tunneling current of 0.1 nA and with bias voltages in the range of 100–300 mV.

Figure 1(a) shows the image of a defect with a diameter of 120 ± 10 nm and a depth of ∼13 nm observed after a voltage jump. This is a typical example of the defects made by either method. In the figure, we can see that the layered structure of 2H-$NbSe_2$ is exposed. The new modulations can appear in the rough area on the edge and the inside of the defect as shown in figures 1(b)–(d). Figure 1(b) focuses on the edge of a 'pit' and the transition from 3×3 to $\sqrt{13} \times \sqrt{13}$ to disorder. Figure 1(c) shows the side of another defect. The new modulation with a lattice constant and corrugation larger than the usual 3×3 modulation is also clearly present in this image. It appears on all the atomic steps which were exposed by the tip–sample interaction. In figure 1(d), taken at the center of a defect, the modulation appeared down to the bottom layers of the defect. Plotted in (e) are the height values along a line cut in (d) marked by the black line. The heights of layers are measured to be 0.65 ± 0.05 nm. The 2H-$NbSe_2$ crystal is composed of stacks of sandwich structures with two Se layers on the outside and one Nb layer on the inside. The bonding between the Se–Nb layers within the sandwich is covalent while the bonding between the stacks is of van der Waals type. The crystal is cleaved between the stacks where the bonding is weak and the Se layers are exposed as the top surface. The height measurement thus indicates that the exposed layers in (d) are all Se surfaces and the distance between the two Se layers is $\frac{1}{2} \times c = 0.636$ nm. Here c is the lattice constant of the crystal in the z direction. Height measurements in (a) and (c) also confirm this result. They are an integer number times of $\frac{1}{2}c$. A simple calculation shows the typical depth of these pits is about 20 stacks. We believe this method is also applicable to other layered materials such as cuprate high-T_c superconductors to create a localized anomaly or expose the lower layers.

To compare the two CDWs, in figure 2(a) we examine the interface. On the left we observed the regular triangular lattice of Se atoms with the signature 3×3 CDW. On the right, the new modulation forms a triangular lattice with a lattice constant of 1.25 nm ($=\sqrt{13}a$, $a = 3.46$ Å) and a rotation of 13.9° relative to the atomic lattice. As shown in figure 2(b) the z deflection from the deep minima to the maxima of the new modulation is much larger (2.1 ± 0.2 Å) than the modulation of the regular 3×3 structure (0.3 ± 0.1 Å) on the left. This large deflection is similar to what was observed on 1T-$TaSe_2$ [4]. It indicates a large charge transfer to the center atoms caused by the new CDW, in contrast to the small charge transfer and z deflection in the 3×3 area. Also similar to 1T-$TaSe_2$ and 1T-TaS_2, the underlying atomic corrugation is difficult to image in this area due to the large $\sqrt{13} \times \sqrt{13}$ corrugation. The atoms at the interface form a rectangular structure as indicated by the superimposed atomic model in figure 2(a). As emphasized by Zhang *et al* [10], the rectangular structure is a natural interface between a 2H and a local 1T stack. Note that the interface of the two CDWs is usually straight and along the lattice directions, but the edges of the defects as illustrated in figure 1 are not. The new modulations on the lower layers could extend to the area underneath the layer on top of it, not just on the area exposed. This observation indicates that the transformation is likely 3D instead of only on the exposed surfaces. The features mentioned above are similar to observations made on 2H-$TaSe_2$ [10]. A pure 1T crystal of $NbSe_2$ does not exist, so there is no experimental data on the electronic and lattice structure of that crystal to compare with our experiment.

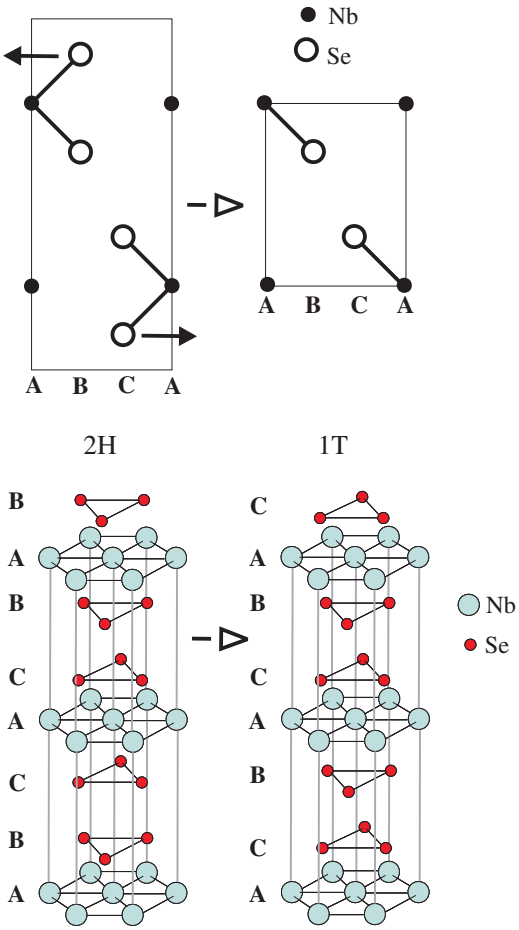

Figure 3. The lattice transition from the 2H phase to the 1T phase. The top diagram shows sections $(11\bar{2}0)$ of the unit cells of the 2H and 1T lattices to illustrate the transition between these phases. The transition happens when the top and bottom Se layers both shift. In the diagram, the top layer shifts from B to C, while the bottom layer shifts from C to B. The bottom graph shows the 3D lattice structures of the two phases to explain the result of the layer shift in real crystals. The first, fourth and fifth layer of Se atoms shift to the corresponding positions.

These observations demonstrate that the impact of the voltage jump or pulse can affect many layers below the surface and probably regions even lower than the bottom layer that is exposed. This new evidence contradicts the top layer shifting scheme proposed by Zhang *et al* [10]. Also, the new CDW appearing on each Se layer suggests that this is a 1T phase of the $NbSe_2$ instead of the 4Hb phase as proposed by Komori *et al* [7]. This is consistent with theoretical calculations [12]. Here we propose a 3D structural transition from 2H to 1T in the area affected by the tip–sample interaction. Figure 3 shows the structural difference of these two phases. During the transition, the top and bottom Se layer of the 2H lattice both shift as illustrated in the figure. Here we use the common notation in the description of close packing structures of an atomic lattice [13]. The top layer shifts from position B to C and the bottom from C to B. The interface of the two lattices with CDWs is visualized in figure 2(a). In what follows, we will refer to the nanosize affected 3D area as the nanocrystal [10].

We speculate that the pulse-generated heating locally transforms the nanocrystal to the 1T phase and the size of the crystal is a result of heat diffusion. It is known that 2H-$NbSe_2$ transforms to a 1T phase at 980 K [14]. Several models have dealt with the steady state temperature of the local heating problem of STM on metal surfaces [15, 16]. In [16] Flores *et al* modeled the dissipation process during tunneling at the tunneling interface. In this model, the energy dissipated through the electron–hole pair excitation channel dominates over the energy through the phonon channel. By balancing the dissipated energy W_{e-h} through the electron–hole pair excitation process and the heat flux carried away by the pairs, the steady state temperature was shown to be $T_s \sim \frac{W_{e-h}}{2\pi r K_s}$. Here $r \sim 5$ Å is the radius of the dissipation region under the tip-end [16]. $K_s \sim K/100$ is the surface thermal conductivity [16], where $K \sim 160$ mW cm^{-1} K^{-1} $= 10^{10}$ eV s^{-1} Å^{-1} K^{-1} is the thermal conductivity of 2H-$NbSe_2$ at 4.2 K [17]. $W_{e-h} \propto V^4$, where V is the pulse/jump voltage. In our experiment, we used $V_{bias} = 3$ mV, $I = 0.1$ nA before the voltage jump. Using a tunneling resistance of $R = 3 \times 10^7$ Ω and jump voltages $V = 5$ and 6 V, we obtained the dissipation power, W_{e-h}, $\sim 2.5 \times 10^{12}$ eV s^{-1} and 5.2×10^{12} eV s^{-1}, respectively. Thus, the steady state temperatures after these two voltage jumps are $T_s \sim 750$ and 1555 K. While this model might not be completely accurate for this situation, it shows that the heating is within the right range. This scheme can also explain the size range of the affected area in Zhang *et al* [10] since the temperature is dependent on V^4 and the size depends strongly on the temperature at the center of the diffusion process. A more sophisticated numerical simulation study such as that for spot welding [11] and the direct measurement of the junction temperature are desirable to understand fully the process of heat generation and clarify the reason behind the creation of the defect. Similar to the spot welding process, the nanocrystal was created by heating and then it was quickly quenched in the 4.2 K environment so the transition became permanent locally. There are also several other possible explanations, however. Mechanical contact was ruled out as we mentioned before. Electron-assisted surface atom sublimation [18] is also not likely because the threshold voltage does depend on the resistance in this case. The sublimation could be part of the process, creating the 'pit' structure but not the nanocrystal.

3. Disordered phase of the new CDW

One interesting aspect is the coexistence of an apparent disordered CDW phase along with the ordered phase as illustrated in figure 4(a). This 97 nm by 97 nm topographic image was taken in an area surrounded by three defects made by voltage pulses. The top defect is partially shown in the image and the left and right defects are outside the field of view. Regions of the modulation that show different orderings are marked by capital letters A–E in figure 4(a) and also in the Fourier transformed image figure 4(b). E is the region where the top layer remains intact and has the atomic and 3×3 CDW signature. It is very easy to identify the ordered regions A, B and C of the $\sqrt{13} \times \sqrt{13}$ modulation in (a) where triangular

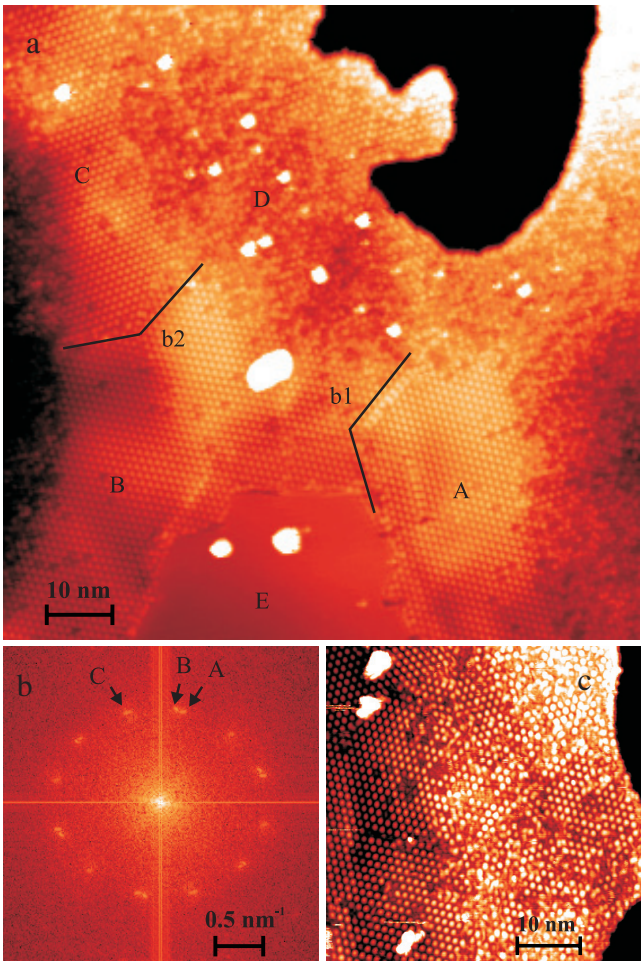

Figure 4. Ordered and disordered phases of the new modulation. (a) Shows a 97 nm × 97 nm scan with different regions identified as different phases of the new modulation. The regions are indicated by A, B, C, D and E, respectively (see the text). b1 and b2 are two domain boundaries that can be easily identified by checking the mismatch of the lattice structures. The image was taken in an area on the surface surrounded by three defects, on the left, right and the top. Only the irregularly shaped defect on the top is partially shown (the dark area). (b) The Fourier transformed image of (a) showing peaks (bright spots) for different ordered regions corresponding to those indicated in (a). (c) Another example of the disordered phase (right) and the ordered phase (left).

lattices with different rotations were formed. This is also a well-known feature of the commensurate phase of the CDW state in 1T systems [8, 19]. The different rotations are clearly shown in the Fourier transformed image (b). We used selective filtering to identify the real-space counterparts of the three groups of six symmetric points in (b). B and C correspond to α-rotated and β-rotated areas where the CDW lattice rotated 13.9° counterclockwise and clockwise respectively relative to the atomic lattice. The rotation of the A phase is 30° more clockwise. This has never been identified in a 1T system. It is not the satellite spot of the incommensurate phase of the CDW in 1T [8] since it has the same wavelength as B and C. Further work is needed to understand the formation of the A phase. The domain sizes of the three phases are of the order of 50 nm^2 which are much smaller than those observed in 1T systems [19]. Due to their small size, we are able to image them all within one scan. Their boundaries are indicated by lines b1 and b2 in figure 4(b). Defects or missing sites of the CDW are also frequently observed as we can see in figure 4(a).

As illustrated in figure 4(a), the disordered region D lies between the ordered regions and the defect. In this region, the ordered periodicity of the modulation is destroyed but the corrugation still has the same amplitude as in the ordered regions. In some areas, the distribution is completely random. The random feature of area D is also captured in figure 4(c) where a 50 nm by 50 nm topographic image of an area close to a pit shows the order/disorder interface. In (c), the disordered region consists of randomly distributed locally ordered plaquettes as compared to D in (a) which has more single 'bubbles' randomly distributed. We believe this could be additional evidence of local heating by the voltage pulse. The radial arrangement of the defect, the disordered phase and ordered phase is an effect of the heat diffusion. The temperature at the center is the highest and enough to remove some material. The next is the disordered phase where the temperature is high enough to melt the CDW phase. The third is the ordered phase where the temperature is above the structural transition temperature but below the melting temperature of CDW. The last circle is the normal 2H region where the temperature is below the structural transition temperature. Since the pulse heating happens quickly and the environment is at 4.2 K, a quenching process similar to that in spot welding of metals [11] likely leaves us the non-equilibrium state of the nanocrystal.

The disorder and the CDW defects suggest the CDW state in this system can be localized. The localization of the CDW was predicted by McMillan on 2H-$TaSe_2$ [20]. In his theory, the coherence length of the localized CDW could be as small as the lattice constant so that the unit cells of the CDW superlattice can be treated as independent local modes with intercell interaction and long range order is broken at the phase transition. This physical picture at the transition is similar to what we observe in area D in figure 4(a) and in figure 4(c). It is unlikely to be caused by impurities or vacancies in the crystal since their uniform distribution would not lead to distinct order and disorder regions. One could argue that the lattice structure near the defect is completely destroyed, but this fails to explain why there still exists local CDWs, i.e. the randomly distributed 'bubbles'. Apparently, more theoretical work and further experiments are needed to study this interesting phase.

4. Periodic structure displacement of the new modulation revealed

The second focus of our observation is the atomic structure of this modulation. As in the 1T case, it is difficult to obtain atomically resolved images of the new modulation [8]. On rare occasions, we have been able to do so, however. Figure 5 shows one of the best such images we have acquired. The tunneling current and bias voltage are 0.1 nA and 100 mV, respectively. The reason we were able to obtain atomic resolution in this image (as compared to figure 2 in which

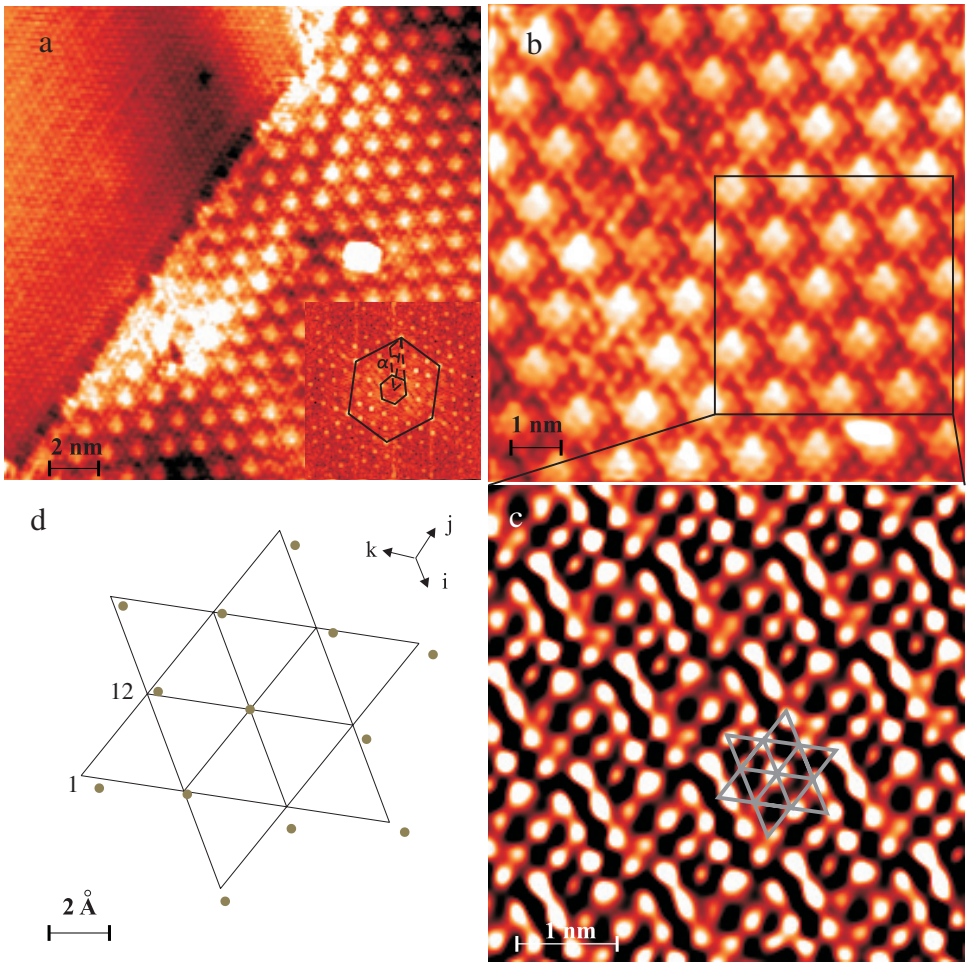

Figure 5. Atomically resolved images. (a) Shows the interface of the 3 × 3 CDW and the $\sqrt{13} \times \sqrt{13}$ CDW. The inset is the Fourier transformed image. Two hexagons are marked. The vertices of the inner hexagon are the corresponding first-order Fourier components of the $\sqrt{13} \times \sqrt{13}$ reconstruction. The vertices of the outer hexagon are the components of the underlying atomic lattice. The 3 × 3 reconstruction on the left in the image is too weak to be shown in the Fourier transformed image, but the pattern can be immediately recognized by eye. The rotation angle α between the hexagons is 13.9° by simple geometry. The geometry also indicates a star-of-David reconstruction with an α-rotation (see section 2). (b) Zooms in on the new modulation part and shows the details of the modulation structure. (c) Shows the underlying atomic lattice by filtering out the CDW ordering in (b). The star-of-David unit cell of the regular lattice centered around a maximum point is also plotted. (d) Shows the measured distortion in a star-of-David unit cell. The regular positions of atoms are plotted by connected lines as in (c). The averaged measured positions are plotted as dots to illustrate the difference. See table 1 for the results of our measurements. Here we keep the same orientation as in (c). $\hat{i}$, $\hat{j}$, $\hat{k}$ are directions of the three CDW vectors in both (c) and (d).

similar parameters were used) is due to the tip state as explained in [8]. Figure 5(a) is a 20 nm by 20 nm topographic image taken at the interface which shows the regular 3 × 3 part on the left and the atomically resolved $\sqrt{13} \times \sqrt{13}$ part on the right. The inset is the Fourier transformed image to illustrate the symmetry of the atomic order (the outside hexagon) and the order of the new modulation (the inside hexagon). Note that the 3 × 3 modulation is very weak compared to the other two so there is no apparent bright spot for it in the Fourier transformed image. From the geometry, we confirm that the new modulation follows the typical symmetry of the CDW in a 1T material [8], a star-of-David reconstruction and in this case an α-rotated phase. A closer look at the real-space image of the new modulation in figure 5(b) reveals the actual construction of this modulation which is quite different from the usual 1T case despite the similarities we have discussed.

In order to reveal the atomic construction of the new modulation, we zoomed into the marked area in (b) where there is no defect in the CDW and removed the Fourier component of the $\sqrt{13} \times \sqrt{13}$ order by Fourier filtering. The real-space image after this process is illustrated in figure 5(c). One feature we can immediately notice is the asymmetry of the distortion of the atomic lattice. To measure the distortion we first processed the image by a center-of-mass method [21] to find the position of each atom. Then we took the atom with highest corrugation (or 'maximum point') of the $\sqrt{13} \times \sqrt{13}$ modulation as the center of the modulation and treated the closest 12 atoms to each center as the other members of the unit cell of the Star-of-David reconstruction. After this, we constructed the regular lattice with no distortion of all the atoms in the image by fixing the positions of the center points. The distortion is calculated as the difference between the measured position of each atom

Table 1. The distortion vectors of the unit cell in figure 5. The atom numbers are from figure 5(d). The error bar is ∼0.08 Å.

Atom	d_i (Å)	d_j (Å)	d_k (Å)	Atom	d_i (Å)	d_j (Å)	d_k (Å)
1	0.62	0.03	0.65	7	0.53	−0.02	−0.51
2	0.14	−0.01	−0.13	8	0.36	0.21	−0.57
3	0.47	−0.25	−0.22	9	0.66	−0.09	−0.57
4	0.77	−0.50	−0.27	10	0.15	0.14	−0.29
5	0.50	0.05	−0.54	11	0.45	0	−0.45
6	0.62	−0.10	−0.51	12	0.05	0.28	−0.34

and the corresponding one on the regular lattice. Each unit cell has 12 distortion vectors for the 12 members except the center. We plotted the averaged results in figure 5(d). The connected lines show the constructed regular lattice and the round dots are the average positions of the other 12 atoms in the unit cell. The atoms are numbered counterclockwise with the first and last one indicated in the plot. The distortions are not symmetric around the center of the cell. The atoms near the interface of the two CDWs are pulled closer, and the atoms near the defect are further apart. This is different from what was observed for CDWs in 1T systems where the distortions are usually symmetric [1]. The asymmetry of the distortion is obviously exposed in the plot.

Table 1 shows the 12 distortion vectors projected on the three CDW wavevectors $\hat{i}$, $\hat{j}$ and $\hat{k}$ ($d_i = \vec{d} \cdot \hat{i}$). The periodic structural displacement (PSD) of the CDW unit cell can be constructed from the 12 distortion vectors around the CDW maxima. Band structure and phase transition calculations using the measured PSD of the CDW [22, 23] could help understand this interesting local phase transition. The result could be compared with further studies of the spectroscopy of the new CDW. From table 1 the largest displacement is 0.8 ± 0.1 Å (24% of the lattice constant) which is anomalously large compared to the distortion observed in usual 1T systems where the maximum displacement $\leqslant$0.2 Å and in 2H systems ($\leqslant$0.05 Å) [24]. The distorted lattice shows the quasi-ribbon-like structure along the direction $\hat{j}$, which is very similar to what was observed in $TaTe_2$ and $NbTe_2$ [1] where large distortions and a ribbon-like structure were observed. We speculate that a single $\vec{q}$ CDW was truncated by the defect in the $\hat{i}$ direction and this caused the asymmetry of the distortion. It also shows that, when there is an asymmetry, the distortion tends to be large as observed in the cases of $TaTe_2$ and $NbTe_2$.

5. Summary

Our scanning tunneling microscopy work at 4.2 K on 2H-$NbSe_2$ shows two distinctive features that have never been reported in related systems. The first is the disordered phase of the new $\sqrt{13} \times \sqrt{13}$ modulation. It shows the CDW can be localized and viewed as individual cells interacting with each other. The second is the large atomic distortion in the new modulation, possibly due to the asymmetry of the nanocrystal. We propose that local heating was the source for nanocrystal creation and the disordered phase was formed by quenching. Further experimental and theoretical studies are necessary to better understand all the phenomena presented in this paper.

Acknowledgments

We would like to thank Dr Danilo Romero at the University of Maryland at College Park and Helmuth Berger at the Institute of Physics of Complex Matter, Switzerland for providing us with the sample.

References

[1] Wilson J A, Di Salvo F J and Mahajan S 1975 Charge–density waves and superlattices in the metallic layered transition metal dichalcogenides *Adv. Phys.* **24** 117–201
[2] Grüner G 1994 *Density Waves in Solids* (Reading, MA: Addison-Wesley)
[3] Wiesendanger R 1994 *Scanning Probe Microscopy and Spectroscopy* (Cambridge: Cambridge University Press)
[4] Coleman R V, Giambattista B, Hansma P K, Johnson A, McNairy W W and Slough C G 1988 Scanning tunnelling microscopy of charge–density waves in transition metal chalcogenides *Adv. Phys.* **37** 559–644
[5] Koslowski B, Xu W, Blackford B and Jericho M H 1996 Observation of a superlattice in silver-intercalated $NbSe_2$ by scanning tunneling microscopy *Phys. Rev.* B **54** 11706–9
[6] Ramšak N, van Midden H J P, Prodan A, Marinković V, Boswell F W and Bennett J C 1999 Defect-induced room-temperature modulation in $NbSe_2$ *Phys. Rev.* B **60** 4513–6
[7] Komori F, Iwaki T, Hattori K, Shiino O and Hasegawa T 1997 New superstructure on the surface of 2H-$NbSe_2$ and tunneling spectra at 4.2 K *J. Phys. Soc. Japan* **66** 298–301
[8] Giambattista B, Slough C G, McNairy W W and Coleman R V 1990 Scanning tunneling microscopy of atoms and charge–density waves in 1T-TaS_2, 1T-$TaSe_2$, and 1T-VSe_2 *Phys. Rev.* B **41** 10082–103
[9] Enss C, Winters R, Reinermann M, Weiss G, Hunklinger S and Lux-Steiner M 1996 STM-study of triangular defect structures induced on WSe_2 *Z. Phys.* B **99** 561–6
[10] Zhang J, Liu J, Huang J L, Kim P and Lieber C M 1996 Creation of nanocrystals through a solid–solid phase transition induced by an STM tip *Science* **274** 757–60
[11] Andrews K T, Guessous L, Nassar S, Putta S V and Shillor M 2006 A one-dimensional spot welding model *J. Appl. Math.* **2006** 1
[12] Kikuchi A and Tsuneyuki S 1998 Electronic structure and charge density wave state in polytypes of $NbSe_2$ *Surf. Sci.* **409** 458–64
[13] Brown B E and Beerntsen D J 1965 Layer structure polytypism among niobium and tantalum selenides *Acta Crystallogr.* **18** 31
[14] Kadijk F and Jellinek F 1971 Polymorphism of $NbSe_2$ *J. Less-Common Met.* **23** 437–41
[15] Li Y Z, Vazquez L, Piner R, Andres R P and Reifenberger R 1989 Writing nanometer-scale symbols in gold using the scanning tunneling microscope *Appl. Phys. Lett.* **54** 1424–6
[16] Flores F, Echenique P M and Ritchie R H 1986 Energy dissipation processes in scanning tunneling microscopy *Phys. Rev.* B **34** 2899–902
[17] Bel R, Behnia K and Berger H 2003 Ambipolar Nernst effect in $NbSe_2$ *Phys. Rev. Lett.* **91** 066602
[18] Kondo S, Heike S, Lutwyche M and Wada Y 1995 Surface modification mechanism of materials with scanning tunneling microscope *J. Appl. Phys.* **78** 155–60
[19] Thomson R E, Burk B, Zettl A and Clarke J 1994 Scanning tunneling microscopy of the charge–density-wave structure in 1T-TaS_2 *Phys. Rev.* B **49** 16899–916

[20] McMillan W L 1977 Microscopic model of charge–density waves in 2H-$TaSe_2$ *Phys. Rev.* B **16** 643–50
[21] Lapshin R V 1998 Automatic lateral calibration of tunneling microscope scanners *Rev. Sci. Instrum.* **69** 3268
[22] Smith N V, Kevan S D and Di Salvo F J 1985 Band structures of the layer compounds 1T-TaS_2 and 2H-$TaSe_2$ in the presence of commensurate charge–density waves *J. Phys. C: Solid State Phys.* **18** 3175–89
[23] McMillan W L 1976 Theory of discommensurations and the commensurate–incommensurate charge–density-wave phase transition *Phys. Rev.* B **14** 1496–502
[24] Wilson J A 1978 Questions concerning the form taken by the charge–density wave and the accompanying periodic-structural distortions in 2H-$TaSe_2$, and closely related materials *Phys. Rev.* B **17** 3880–98